RSC Advances

ROYAL SOCIETY OF CHEMISTRY

www.rsc.org/advances

Protein conjugated carboxylated gold@reduced graphene oxide for aflatoxin B_1 detection

Saurabh Srivastava[a,b,c], Shiju Abraham[b], Chandan Singh[a], Md. Azahar Ali[a], Anchal Srivastava[b], Gajjala Sumana[a], Bansi. D. Malhotra[a,c*]

[a]Department of Science and Technology, Center on Biomolecular Electronics, Biomedical Instrumentation Section, CSIR-National Physical Laboratory, New Delhi-110012, India
[b]Department of Physics, Banaras Hindu University, Varanasi, U.P.-221005, India
[c]Department of Biotechnology, Delhi Technological University, Delhi-110042, India

ABSTRACT

A sensitive, reproducible, stable and label-free immunosensor has been demonstrated via simultaneous reduction of graphene oxide and gold (III) salt using eco-friendly and non-toxic reducing agent sodium citrate resulting in uniformly distributed gold nanoparticles onto the reduced graphene oxide (rGO) sheets. The *in-situ* grown gold @ carboxylated reduced graphene oxide(Au@rGO) surface has been used for bioconjugation with monoclonal antibodies of aflatoxin B_1 using EDC-NHS chemistry. The *in situ* grown AuNPs into rGO sheet results in improved electrocatalytic activity and loading of the antibodies due to the enhanced surface area. The monodispersion of Au nanoparticles on rGO sheets yields heterogeneous electron transfer (2.85×10^{-4} cm s^{-1}) resulting in improved biosensor efficacy compared to that based on rGO electrode. This immunosensor is sensitive to 0.1 ng/mL concentration of aflatoxin compared to the reported ELISA standard method. The Au@rGO based immunosensor exhibits high sensitivity (182.4 μA/(ng/mL)/cm^2) in a wide linear detection range of 0.1-12 ng/mL. Results of the studies related to this immunosensor reveal that Au@rGO nanocomposite is a suitable platform for the development of compact biosensing device for food toxins monitoring.

Keywords: Reduced graphene oxide, Gold nanoparticles, Aflatoxin, Immunosensor, Label-free detection.

***Corresponding Author: Email:** bansi.malhotra@gmail.com, **Phone:** 91-11-27871043 (Ext-1609)

INTRODUCTION

Graphene, a single layer of sp^2 hybridized carbon atoms resembling honeycomb lattice, is the fundamental building block of all carbonaceous nanomaterials. It is in increased demand owing to its unique electrical, optical and mechanical properties. [1-4] The reduced graphene oxide (rGO) synthesized by chemical method has recently aroused much interest as an excellent candidate for biosensing application. The abundant functional groups (hydroxyl and epoxies at the basal plane while carboxyl groups at edges), larger surface area, capability to facilitate direct electron transfer from the enzymes and proteins, ease of processing and low cost reveal rGO as an interesting candidate as compared to that of pristine graphene for electrochemical biosensing. [5-7] The oxygenated functional groups present in rGO have been found to be responsible for the heterogeneous charge transfer resulting in faster electron transfer kinetics.[6] Moreover, the oxygenated functional groups present in rGO facilitate direct covalent attachment of desired biomolecules onto rGO surface providing high stability to the biosensor.

Compton et al. have recently reported chemically active reduced graphene oxide (rGO) with a considerable amount of functional groups suitable for biomolecules attachment and with desired conductivity for electrochemical sensing applications. [8] The rGO based materials have been employed for enzymatic analysis, genosensor development and food toxin detection etc. [9-16] Although rGO has been utilized in many electrochemical biosensing applications, there is a considerable scope to improve the biosensing characteristics such as sensitivity, detection limit and stability. In this context, the nanocomposite of rGO with metal nanoparticle [17-19], metal oxide nanoparticle [20-21]and conducting polymers [22-23] for biosensing applications have recently aroused much interest.

The functionalization of rGO with the noble metals such as gold (Au) and platinum (Pt) has been employed for development of high performance electrochemical biosensing devices.[24-27] The noble metal nanoparticles are known to possess excellent electrocatalytic properties and the resulting Au@rGOnanocomposite has been found to exhibit enhanced voltammetric current as compared to that of the bare rGO. Moreover, the high surface area and oxygenated moieties of rGO provide an efficient support for homogeneous dispersion of metal nanoparticles without affecting their electrochemical activities. Chen et al. have reported gold-graphene nanohybrid for electrochemical detection of glucose with 400-fold enhanced sensitivity as compared to that of rGO. [27] Guo et al. have demonstrated that the platinum nanoparticles-graphene hybrid nanosheets

show higher voltammetric current and can be used to detect several organic and inorganic molecules with superior sensitivity in comparison to those based on graphene. [25]

Aflatoxins (AF) are a group of secondary fungal metabolites that are produced by *Aspergillus flavus and Aspergillus parasiticus* under certain conditions and are the most widely spread group of toxins resulting in contamination of food products. Among these, aflatoxin B_1 (AFB_1) is known to be the most toxic and is responsible for human hepatocellular carcinoma (International Agency for Research on Cancer regards it as a human carcinogen). [28-29] Thus, sensitive and efficient detection of this food toxin is urgently needed to monitor food safety and human health. In this context, the development of an electrochemical biosensor has recently aroused much interest due to its high sensitivity, fast detection and simplicity. We have recently reported rGO based immunosensor for the detection of food toxin[9].

We report *in situ* fabrication of Au@rGOnanocomposite via simultaneous reduction of GO and Au^{3+}. This Au@rGOnanocomposite material has been used as a sensitive platform for electrochemical detection of food toxin (aflatoxin B_1). The proposed electrochemical detection strategy offers higher sensitivity, improved detection range and stability. The sodium citrate acts as capping reagent for the effective reduction and stabilization of Au@rGOnanocomposite.[27, 30] Sodium citrate is considered to be a non-toxic reducing agent as compared to hydrazine/sodium borohydride that is known to be highly toxic and explosive, for the reduction of rGO. Moreover, unlike rGO tailored via hydrazine that is known to agglomerate, rGO obtained via sodium citrate is found to form stable colloidal dispersion due to hydrogen bonds between the oxygenated functional groups on the surface of rGO and the hydroxyl/carboxyl groups of sodium citrate. [30] Moreover, these functional groups render enhanced biomolecules loading for biosensing application. To the best of our knowledge, this is the first report towards the application of *in situ* derived carboxylated Au@rGO nanocomposite based platform for the food toxin detection.

RESULTS AND DISCUSSION

Electron microscopy studies

Transmission electron micrograph (TEM) of GO shows good quality and thin layered graphene dispersed on carbon coated copper grid [(Fig. 2 (i)]. It can be clearly seen that the wrinkles and folds (marked region) appear on the GO sheet due to defects and functional groups in the carbon lattice. It appears that the GO sheet is extended to several micrometers and the

dark region corresponds to the multilayered GO. The TEM image of Au@rGO nanocomposite is shown in Fig. 2(ii) wherein monodispersed Au nanoparticles (Au NPs) are clearly visible on the rGO surface. The rGO sheets possess defects and residual oxygenated functional groups that perhaps act as the nucleation sites for Au NPs formation. The atomic scale image of Au NP shows clear lattice fringes. The average inter-planar spacing of lattice fringes is found to be 2.35 Å corresponding to (111) plane [Fig. 2(iii)] which is in good agreement with results of the X-ray diffraction studies. Fig. 2(iv) shows particle size distribution of the Au NPs present at the rGO surface.

The surface morphology of the various modified electrodes has been investigated using scanning electron microscopy (SEM) as depicted in Fig.3. Image (i) shows SEM of the rGO where the graphene sheets are found to be several microns in dimension. It appears that the rGO sheest stack together to form larger sheet during coherent deposition on ITO electrode. However, morphology of the Au@rGO /ITO electrode [image (ii)] reveals that Au grains are incorporated throughout the rGO sheet. Some Au NPs are visible on the surface of the graphene sheets while some of them are found to be entrapped between the rGO sheets as clearly visible in the enlarged image (iii). However, after antibody functionalization, the surface morphology of the Au@rGO /ITO electrode completely changes due to the high antibodies loading on electrode surface [image (iv)].

Structural studies

Fig.4 (i) shows the UV-visible spectra of (a) GO, (b) rGO and (c) *in-situ* synthesized Au@rGO nanocomposite dispersed in water. UV-visible spectrum of GO shows absorption peak at 232 nm due to π-π* transition of aromatic C–C bonds. However, after rGO formation the maximum absorption peak is found to be red shifted to 270 nm indicating reduction of GO. [9] The Au NPs exhibit the characteristic absorption peak at 530 nm (inset; Fig.4). The *in situ* synthesized Au@rGO nanocomposite shows two absorption peaks at 270 nm and 530 nm. This result indicates simultaneous reduction of Au^{3+} to Au as well as GO to rGO leading to Au@rGO nanocomposite formation.

Fig. 4 (ii) shows XPS spectrum of C 1s region of the Au@rGO nanocomposite. The spectrum has been deconvoluted into the characteristic binding energy peaks using peak fit 1 software. Background subtraction and peak fitting of the spectra have been done using the

Shirley function and Gaussian function, respectively. XPS measurements have been carried out in a Perkin Elmer XPS chamber (PHI 1257) with a base pressure of 5×10^{-9} torr. The chamber is equipped with a dual anode comprising of Mg-K_α (energy 1253.6 eV) and Al-K_α (energy 1486.6 eV) X-ray source and a high-resolution hemispherical energy analyzer for energy resolved electron detection. An Mg-K_α X-ray source has been used for this study. The samples are sputtered with 4 keV arGOn ions to remove surface contamination prior to XPS studies. The binding energy peak found at 284.5 eV is assigned to graphitic C-C. Peak found at 285.5 and 286.7 eV is due to the hydroxyl (C-OH) and epoxy (C-O) groups, respectively. Further, the binding energy peak seen at 288.2 and 289.4 eV can be attributed to the carbonyl (C=O) and carboxylic acid (O-C=O) groups present in the samples. Table 2 indicates the binding energy position of the various functional groups, FWHM and the corresponding relative percentage of these groups in the Au@rGO nanocomposite. These results indicate that the Au@rGO nanocomposite has abundant carboxylic acid functional groups as evident by their high relative atomic percentage (10.4 %). These carboxylic acid groups have been used to bind with amino terminal of the antibodies through the covalent immobilization process.

Fig.4 (iii) shows Fourier transform infrared spectra (FT-IR) of (i) rGO/ITO (ii) Au@rGO /ITO and (iii) anti-AFB_1/Au@rGO /ITO films. The rGO and Au@rGO exhibits the characteristic peak at 1413 cm^{-1} corresponding to O–H bending vibration of the carboxyl group. The band seen at around 1600 cm^{-1} is due to aromatic C=C stretching vibration. The broad band found at around 3300 may be assigned to O-H stretching. Further, the band found in the region of 1000-1143 cm^{-1} corresponds to C-OH stretching vibration. In the FT-IR spectrum of anti-AFB_1/ Au@rGO /ITO film (spectrum iii), it may be noted that intensity of the 1413 cm^{-1} band (corresponds to O–H bending vibration of the carboxyl group) is considerably reduced as compared to that of the Au@rGO /ITO film (spectrum ii). An additional peak corresponding to amide I appears at 1664 cm^{-1}. This indicates that carboxylic acid groups present in the nanocomposite have been utilized in the amide bond formation with amino groups of the antibodies. The band seen at 3300 cm^{-1} becomes much broader and is shifted to 3400 cm^{-1} due to presence of the amide N-H stretching vibrations in the antibodies.

Fig. S1 (see Supplementary Information sheet) shows X-ray diffraction (XRD) pattern of electrophoretically deposited Au@rGO film on ITO substrate. The XRD pattern exhibits characteristic peaks corresponding to rGO, Au and ITO. A broad hump observed at $2\theta=25^o$

represents the characteristic (002) plane ($d_{002=}$ 3.56 Å) of RGO. [31]. The characteristic peak occurring at 38^o is assigned to (111) reflection plane (d_{111} =2.36 Å) of the fcc gold. Another peak seen at 44^o corresponds to (200) plane (d_{200} =2.05 Å) of Au (JCPDS 89-3697). Rest of the XRD peaks seen at 21.2^o, 30.2^o, 35.1^o and 50.6^o may be assigned to (211), (222), (400) and (440) reflection planes, respectively, arising due to the ITO substrate (JCPDS 89-4596). The crystallite size of Au NPs has been estimated to be as 26 nm using the Debye–Scherrer equation.

Electrochemical studies

Fig.5 (i) shows cyclic voltammograms (CV) obtained for the various modified electrodes at 30 mV/s scan rate obtained using a three electrode system in phosphate buffer saline (PBS) at pH 7.4 containing 5mM $[Fe(CN)_6]^{3-/4-}$. It can be seen that magnitude of the oxidation peak current of rGO/ITO electrode (255 µA) is higher as compared to that of the GO/ITO electrode. This is attributed to the higher conductivity of rGO arising from reduced functional group and defects compared to that of GO (curve a-b). Additionally, the peak-to-peak separation of rGO/ITO is found to be smaller as compared to that of the GO/ITO electrode indicating faster electron transfer. Moreover, *in situ* synthesized rGO-Au/ITO electrode exhibits 3-fold enhanced current (576.7 µA) indicating that decoration of rGO with Au nanoparticles increases the electroactive surface area providing the conducting bridges for the electron-transfer. Alternately, it may perhaps be attributed to the metallic conductivity as well as excellent electrocatalytic activity of gold nanoparticles decorated rGO. After antibody functionalization, the oxidation current is found to decrease (468.4 µA) and peak potential is shifted to more positive value. This indicates insulating nature of the immobilized antibody molecules. The anodic peak current further decreases to 335 µA in case of the BSA/anti-AFB_1/Au@rGO /ITO electrode. This is due to the fact that BSA blocks most of the non-specific active sites present on the immunoelectrode surface. The electrochemical surface area [32] is related to the charge associated with a known adsorbate ($[Fe(CN)_6]^{3-/4-}$) on the electrode surface (ITO), q_m, and the charge associated with that of the various modified electrode (monolayer coverage of the said adsorbate), q_{ad} as

$$A_{ec} = q_{ad}/q_m \quad (1)$$

It has been found that the electrochemical surface area increases significantly in case of the Au@rGO/ITO electrode (137 mm^2) as compared to that of the rGO/ITO (36.5 mm^2) and GO/ITO (29.4 mm^2) electrode. This indicates that Au@rGO exhibits higher electrochemical

surface area leading to the large scale redox conversion of $[Fe(CN)_6]^{3-/4-}$ and enhanced CV response.

Fig.5 (ii) shows CV response of four nanocomposite electrodes as a function of $HAuCl_4 \cdot 3H_2O$ concentration. The concentration of rGO has been taken as 1 mg/mL for all the four fabricated electrodes whereas the loading amount of Au NPs on the rGO sheet has been controlled by taking different concentration of $HAuCl_4 \cdot 3H_2O$ [0.2 mg/mL or 0.5 mM for Au@rGO 1, 0.4 mg/ mL or 1 mM for Au@rGO and 0.8 mg/mL or 2 mM for Au@rGO2]. It has been observed that the redox peak current increases with increasing Au loading on rGO sheet [Fig.S2 (ii)]. It is attributed to the increased electrochemical surface area and conductivity due to the increased amount of Au NPs. The concentration of the gold salt directly influences the size of the synthesized AuNPs that has a strong relationship with the electrochemical performance of the fabricated immunosensor. Ahmad *et al.* have concluded that increasing the concentration of gold salt results into the large size AuNPs with agglomerated geometry while low concentration results into the smaller AuNPs.[33] In our case with increase in the concentration from 0.2 mM to 0.4 mM , current exihibits significant increase and after which it becomes saturated due to large agglomerated AuNPs. Keeping this in view, 0.4 mM of gold salt has been utilized for immunosensor fabrication.

Fig. S2 (i) (see Supplementary Information sheet) shows cyclic voltammograms of the BSA/anti-AFB_1/ Au@rGO /ITO immunoelectrode obtained as a function of scan rate (30–100 mV/s). It has been observed that redox peak current as well as potential increase linearly with square root of the scan rate. This indicates that the redox reaction is controlled by semi-infinite linear diffusion resulting in faster electron transfer kinetics. The slope and intercept follow Equations (2-5):

$$I_a[A] = 4.06 \times 10^{-5}[A] + 4.4 \times 10^{-5}[A^2 s/mV]^{1/2} \times \{scan\ rate\ (mV/s)\}^{1/2};\ R^2 = 0.99 \quad (2)$$

$$I_c[A] = -8.4 \times 10^{-5}[A] - 3.3 \times 10^{-5}[A^2 s/mV]^{1/2} \times \{scan\ rate\ (mV/s)\}^{1/2};\ R^2 = 0.99 \quad (3)$$

$$V_{ap} = 7.4 \times 10^{-2}(V) + 1.7 \times 10^{-2}(V^{1/2}s^{-1/2}) \times \{scan\ rate\ (mV/s)\}^{1/2};\ R^2 = 0.98 \quad (4)$$

$$V_{cp} = -1.2 \times 10^{-1}(V) - 1.4 \times 10^{-2}(V^{1/2}s^{-1/2}) \times \{scan\ rate\ (mV/s)\}^{1/2};\ R^2 = 0.99 \quad (5)$$

The surface coverage of the BSA/anti-AFB_1/Au@rGO/ITO immunoelectrode has been estimated to be as 3.96×10^{-8} mol/cm^2 using Brown–Anson Model. [34]

Fig. S2 (ii) (see Supplementary Information sheet) shows electrochemical impedance spectra (EIS, Nyquist plots) of different modified electrodes in the frequency range of 10^4 to 10^{-1} Hz at a biasing potential of 10 mV. The electrochemical system can be modeled by an equivalent circuit (Randles circuit) comprising of the solution resistance (R_S), charge transfer resistance (R_{CT}), Warburg impedance (W) and double layer capacitance (C_{DL}) etc. The charge transfer process in this electrode has been investigated by measuring the charge transfer resistance (R_{CT}) that depends on the dielectric characteristics at the electrode/electrolyte interface. The R_{CT} value of rGO/ITO electrode is found maximum as 721 Ω. However, the significant reduction in the R_{CT} value observed in the case of Au@rGO/ITO electrode (136 Ω) may be attributed to the higher conductivity as well as excellent electrocatalytic activity of Au nanoparticles in the nanocomposite matrix. The antibody functionalized matrix (anti-AFB_1/Au@rGO/ITO) exhibits higher R_{CT} (179 Ω) as compared to that of the Au@rGO/ITO and is attributed to insulating nature of the antibody molecules. Further, since BSA molecules cover most of the non-specific active sites of the immunoelectrode surface, the charge transfer process is again hindered, resulting in higher R_{CT} (448 Ω) in case of BSA/anti-AFB_1/Au@rGO/ITO electrode.

The heterogeneous electron transfer rate constant (k_0) of Au@rGO /ITO and rGO/ITO electrode has been calculated using Eq. 6 [35]

$$k_0 = \frac{RT}{n^2F^2AR_{CT}S} \quad (6)$$

where R is gas constant, T is absolute temperature (K), F is Faraday constant, A is the specific electrode area (cm^2), S is the bulk concentration of redox probe (mol cm^{-3}) and n is the number of transferred electrons per molecule of the redox probe. The k_0 value of the Au@rGO/ITO electrode has been estimated as 2.85×10^{-4} cm s^{-1} that is better than that of a rGO/ITO electrode (2.02×10^{-4} cm s^{-1}). This indicates that the Au@rGO/ITO electrode exhibits faster electron transfer kinetics as compared to that of rGO leading to superior analytical performance of the biosensor.

Electrochemical response studies

Fig.6 (i) demonstrates results of the electrochemical sensing studies related to the BSA/anti-AFB_1/Au@rGO /ITO immunoelectrode as a function of AFB_1 concentration (0.1–12 ng mL^{-1}) in PBS (pH 7.4) containing 5mM $[Fe(CN)_6]^{3-/4-}$. It has been observed that magnitude of the peak current decreases as a function of AFB_1 concentration in the detection range, 0.1-12

ng/mL after which it saturates. The reduction in response current may be attributed to the formation of electrically insulating antigen-antibody complex produced from specific interaction of the aflatoxin B1 and antibodythat may block the electron transfer via $[Fe(CN)_6]^{3-/4-}$. [36] Fig. 6(ii) exhibits the calibration plot relating to the change in the magnitude of anodic peak current of BSA/anti-AFB_1/Au@rGO/ITO immunoelectrode as a function of AFB_1 concentration in the detection range of 0.1-12 ng/mL (curve a). Furthermore, a control experiment has been performed to check cross reactivity of the BSA/Au@rGO/ITO electrode with the AFB_1 antigens in absence of antibodies (curve b, Fig. 6(ii)). However, no significant change in the current response has been observed for BSA/Au@rGO/ITO electrode as a function of AFB_1 concentration. This indicates that the AFB_1 only interact with BSA/anti-AFB_1/Au@rGO/ITO immunoelectrode resulting change in the CV response. It has been found that the current varies proportionally with the logarithmic AFB_1 concentration in the linearity range of 0.1-12 ng/mL according to Eq.7

$$I_p = 2.7 \times 10^{-4} - 4.56 \times 10^{-5} log[AFB_1\ concentration\ (ng\ mL^{-1})]\ ;R^2 = 0.992 \qquad (7)$$

The sensitivity of the immunosensor after incorporation of Au NPs by *in situ* reduction method has been estimated as 182.4 μA/(ng/mL)/cm^2 which is found to be improved as compared to that of the rGO/ITO based biosensor (68 μA/(ng/mL)/cm^2).[9] This is attributed to the high electrocatalytic activity and larger electrochemical area of Au decorated rGO matrix. Further, the wider linearity range (0.1-12 ng/mL) of Au@rGO/ITO is due to high loading of antibody molecules to the rGO sheet as well as to the surface of Au. While for rGO/ITO electrode, linearity is only 0.25-1.25 ng/mL [9] [Table 1]. This immunosensor can be used to detect AFB_1 concentration as low as 0.1 ng/mL in solution.

Fig. 7 (i) shows CV response of the BSA/anti-AFB_1/Au@rGO/ITO immunoelectrode in the presence of AFB_1 (1ng/mL) obtained at a regular interval of 1 week. It has been found that the current value decreases to 2.32 % after 8 weeks. This indicates that the fabricated BSA/anti-AFB_1/ Au@rGO/ITO immunoelectrode exhibits good stability at least for two months.

Fig. 7 (ii) indicates CV response of five different BSA/anti-AFB_1/ Au@rGO /ITO immunoelectrodes fabricated using similar procedure in presence of AFB_1 (1 ng/mL) concentration. The relative standard deviation (RSD) of reproducibility for these electrodes is estimated to be as 2.32 % indicating good reproducibility and precision. The electrochemical

sensing performance of this BSA/anti-AFB_1/ Au@rGO /ITO based immunosensor for AFB_1 detection has been compared with those reported in literature (Table 1).

EXPERIMENTAL

Materials

Gold (III) chloride trihydrate ($HAuCl_4 \cdot 3H_2O$; purity 99.99 %), aflatoxin B_1 (AFB_1), anti-aflatoxin B_1 mouse monoclonal antibodies (anti-AFB_1) and bovine serum albumin (BSA) have been purchased from Sigma-Aldrich USA. Graphite flakes (NGS Naturgraphit GmbH, Germany), tetra ethyl ortho-silicate (TEOS, Aldrich, purity ≥ 99% with trace metal basis), H_2SO_4, H_3PO_4, $KMnO_4$, H_2O_2, ammonia solution, ethanol, etc. are of technical grade. Deionized water has been used in all the buffer and solution preparation.

Synthesis of graphene oxide

The graphene oxide (GO) has been synthesized by a method proposed by Marcano *et al.* [37] Briefly, 9: 1 combination of concentrated H_2SO_4 / H_3PO_4, (240ml /26.7ml) has been added to 2 gms of graphite flakes and 12 gms of $KMnO_4$. $KMnO_4$ is mixed within 15 min in order to avoid any explosion, since the above mixing process is exothermic in nature. After that the reaction is subjected to magnetic stirring for 12 h at a temperature of 50° C. This reaction is subsequently quenched by adding about 270 ml of ice with 2ml of 30% H_2O_2. The yellowish slurry mixture is then shifted, centrifuged and filtered. The filtrate thus obtained is washed with 30% HCl and subsequently with distilled water until the pH ~7 and is dried at 70°C to obtain solid GO.

Synthesis of reduced graphene oxide

The graphene oxide is converted into reduced graphene oxide (rGO) using sodium citrate. 10 ml (1mg/ml) of highly dispersed aqueous suspension of GO is added with 100 mg of sodium citrate and the solution is subjected to stirring for about 4 h at 60° C. The colour of the solution changes from brown to black indicating conversion of GO to rGO. After the solution is cooled to room temperature the resultant homogeneous dispersion is centrifuged at 12000 rpm and washed with Milli-Q water. Subsequently, the rGO is re-dispersed into 10 mL water for further characterization.

In-situ synthesis of Au@rGO nanocomposite

100 mg of sodium citrate is added to 10 mL (1mg/mL) aqueous suspension of GO and the solution is refluxed for 3 h at 60 °C. Further 1 mL of $HAuCl_4 \cdot 3H_2O$ (10mM) is added to the above solution and reflux is continued for another 1 h. Finally, the resulting homogeneous dispersion is centrifuged at 12000 rpm and washed with Milli-Q water. Subsequently, the nanocomposite material (Au@rGO) is re-dispersed in 10 mL acetonitrile that has been used as stock solution for the electrophoretic deposition.

Fabrication of RGO-Au/ITO electrodes

Au@rGO nanocomposite film is deposited onto ITO substrate using the electrophoretic deposition (EPD) technique. 100 µL of the stock solution of Au@rGO is re-dispersed in 10 mL of acetonitrile to prepare the colloidal suspension. A constant DC voltage source having two electrode systems is used for EPD. Pre-cleaned ITO coated glass substrate (sheet resistance $30\Omega cm^{-1}$) and platinum foil are used as anode and cathode, respectively. 10^{-4} mol of magnesium nitrate [Mg $(NO_3)_2.6H_2O$] is taken as an electrolyte in the colloidal suspension that imparts surface charges to Au@rGO nanocomposite for the uniform film deposition. [38] The electrodes having separation of 1 cm are immersed into the colloidal suspension containing Au@rGO and subjected to constant electric field (100 V/cm) for 90 s. The fabricated Au@rGO /ITO electrodes ($0.25cm^2$), are removed from the suspension and dried.

Immobilization of monoclonal antibodies onto RGO-Au/ITO electrodes

Monoclonal anti-aflatoxin B_1 (anti-AFB_1) antibody solution (10µg/mL) is freshly prepared in phosphate buffer (PB, pH 7.4). Prior to antibody functionalization, the carboxyl group present on the Au@rGO /ITO electrode is activated using EDC-NHS chemistry. [39]

10 µL of the antibody solution is uniformly cast onto Au@rGO /ITO electrode surface and is incubated for 4 h under humid conditions at room temperature. It is then washed with bovine serum albumin (BSA) solution (0.1mg/mL) prepared in PB. BSA is used to block non-specific active sites present on the immunoelectrode surface. The BSA-anti-AFB_1/ Au@rGO /ITO bioelectrode is then washed with PB and stored at 4°C, when not in use. Fig. 1 demonstrates the fabrication of the carboxylated Au@rGO nanocomposite electrodes and its antibody functionalization strategy.

Characterization

The synthesized Au@rGO has been characterized by X-ray diffraction (XRD, Rigaku) and UV-visible (Perkin-Elmer). The structural and morphological characterizations are carried

out using scanning electron microscopy (SEM LEO 440) and transmission electron microscopy (TEM, Tecnaii-G2F30 STWIN). XPS measurements have been carried out in a Perkin Elmer XPS chamber (PHI 1257) with a base pressure of 5×10^{-9} Torr. An Mg-Kα X-ray source has been used for this study. The chemical structure of Au@rGO is investigated by Fourier transformed infra-red spectroscopy (FT-IR, Perkin-Elmer, model spectrum BX). Electrochemical studies such as cyclic voltammetry (CV) and electrochemical impedance spectroscopy (EIS) are conducted using Autolab, Potentiostat/Galvanostat (AUT-84275). The electrochemical studies have been carried out using three electrode systems where ITO is working, platinum (Pt) as counter electrode and Ag/AgCl as reference electrode.

CONCLUSION

We have demonstrated a uniformly dispersed Au nanoparticles on rGO sheets platform for aflatoxin detection with and without antibody conjugation. The Au@rGO nanocomposite has been fabricated onto ITO electrode and subsequently functionalized with monoclonal anti-AFB_1. Sodium citrate helps in the simultaneous reduction of gold ions onto graphene sheets. The XPS and FT-IR analysis confirm the carboxylated nature of Au@rGO sheets desirable for covalent interaction with antibody via strong amide bond leading to higher stability and low detection limit. It has been found that incorporation of Au nanoparticles at rGO results in enhanced electrochemical activity and heterogeneous electron transfer rate as compared to the bare rGO. The shape, size, distribution and crystalline structure of Au@rGO have been investigated by electron microscopic, spectroscopic and optical techniques. The analytical performance of this immunosensor has been investigated by electrochemical technique. The biosensor shows a higher sensitivity of 182.4 $\mu A/(ng/mL)/cm^2$, an extended linearity of 0.2-12 ng/mL and a good storage stability of 8 weeks alongwith high reproducibility. It should be interesting to use this novel bioelectrode for detection of other food toxins such as aflatoxin M_1, ochratoxin-A, etc.

ACKNOWLEDGEMENTS

We thank Prof. R. C. Budhani, Director, CSIR-National Physical Laboratory, New Delhi, India for providing the facilities. C.S. and Md. A. A. are thankful to the Council of Scientific and Industrial Research, India for providing senior research fellowships. S.S. acknowledges University Grant Commission, India for providing Dr. D. S. Kothari Postdoctoral fellowship.

The financial support received from Department of Science and Technology, India (Grant No. DST/TSG/ME/2008/18) and Indian Council of Medical Research, India (Grant No. ICMR/5/3/8/91/GM/2010-RHN) is gratefully acknowledged.

Table 1: Response characteristics of the BSA/anti-AFB1/ Au@rGO /ITO based biosensor along with those reported in literature.

Bioelectrode	**Sensitivity μA/(ngmL^{-1})/cm^2**	**Detection limit (ng/mL)**	**Detection range (ng/mL)**	**Stability (days)**	**Ref**
BSA-anti-AFB_1/MWCNTs/ITO	95	0.08	0.25-1.375	42	[34]
BSA-*anti*-AFB_1/ RGO/ITO	68	0.15	0.125-1	45	[9]
BSA-*anti*-AFB_1/Ni-ITO	59	0.327	0.05-1	60	[40]
BSA/aAFB1-C-AuNP/MBA/Au	45	0.18	0.1–1	-	[41]
BSA-AFB_1/PTH/Au NP/GCE	1.23	0.07	0.06-2.4	-	[42]
96-wellscreen printed microplate	-	0.03	0.05-2	30	[43]
BSA/*anti*-AFB_1/ Au@rGO /ITO	182.4	0.1	0.1-12	56	Present work

Table 2: The various functional groups, their binding energy position, FWHM and the relative percentage of these functional groups.

Functional groups	Binding energy position (eV)	FWHM (eV)	Relative percentage (%)
C-C	284.4	1.3	53.7
C-OH	285.5	1.35	20.2
C-O	286.7	1.35	10.2
C=O	288.2	1.58	5.6
O-C=O	289.4	2.6	10.3

References

1. A. K. Geim and K. S. Novoselov, *Nature materials*, 2007, 6, 183-191.
2. G. Brumfiel, *Nature*, 2009, 458, 390.
3. K. P. Loh, Q. Bao, G. Eda and M. Chhowalla, *Nature chemistry*, 2010, 2, 1015-1024.
4. C. Xu, X. Wang and J. Zhu, *The Journal of Physical Chemistry C*, 2008, 112, 19841-19845.
5. D. Chen, H. Feng and J. Li, *Chemical Reviews*, 2012, 112, 6027-6053.
6. M. Pumera, *Chemical Society Reviews*, 2010, 39, 4146-4157.
7. M. Pumera, *Materials Today*, 2011, 14, 308-315.
8. O. C. Compton, B. Jain, D. A. Dikin, A. Abouimrane, K. Amine and S. T. Nguyen, *ACS Nano*, 2011, 5, 4380-4391.
9. S. Srivastava, V. Kumar, M. A. Ali, P. R. Solanki, A. Srivastava, G. Sumana, P. S. Saxena, A. G. Joshi and B. Malhotra, *Nanoscale*, 2013, 5, 3043-3051.
10. C. Shan, H. Yang, J. Song, D. Han, A. Ivaska and L. Niu, *Analytical Chemistry*, 2009, 81, 2378-2382.
11. M. Zhou, Y. Zhai and S. Dong, *Analytical Chemistry*, 2009, 81, 5603-5613.
12. A.-M. J. Haque, H. Park, D. Sung, S. Jon, S.-Y. Choi and K. Kim, *Analytical Chemistry*, 2012, 84, 1871-1878.
13. Y. Wan, Z. Lin, D. Zhang, Y. Wang and B. Hou, *Biosensors and Bioelectronics*, 2011, 26, 1959-1964.
14. R. K. Srivastava, S. Srivastava, T. N. Narayanan, B. D. Mahlotra, R. Vajtai, P. M. Ajayan and A. Srivastava, *ACS Nano*, 2011, 6, 168-175.
15. R. S. Dey and C. R. Raj, *The Journal of Physical Chemistry C*, 2010, 114, 21427-21433.
16. S. Alwarappan, C. Liu, A. Kumar and C.-Z. Li, *The Journal of Physical Chemistry C*, 2010, 114, 12920-12924.
17. T. Liu, H. Su, X. Qu, P. Ju, L. Cui and S. Ai, *Sensors and Actuators B: Chemical*, 2011, 160, 1255-1261.
18. S. Mao, G. Lu, K. Yu, Z. Bo and J. Chen, *Advanced materials*, 2010, 22, 3521-3526.
19. T. T. Baby, S. Aravind, T. Arockiadoss, R. Rakhi and S. Ramaprabhu, *Sensors and Actuators B: Chemical*, 2010, 145, 71-77.
20. J. Xu, C. Liu and Z. Wu, *Microchim Acta*, 2011, 172, 425-430.
21. T. Kavitha, A. I. Gopalan, K.-P. Lee and S.-Y. Park, *Carbon*, 2012, 50, 2994-3000.
22. X. M. Feng, R. M. Li, Y. W. Ma, R. F. Chen, N. E. Shi, Q. L. Fan and W. Huang, *Advanced Functional Materials*, 2011, 21, 2989-2996.
23. Y. Bo, H. Yang, Y. Hu, T. Yao and S. Huang, *Electrochimica Acta*, 2011, 56, 2676-2681.
24. W. Hong, H. Bai, Y. Xu, Z. Yao, Z. Gu and G. Shi, *The Journal of Physical Chemistry C*, 2010, 114, 1822-1826.
25. C. Zhu, S. Guo, Y. Fang and S. Dong, *ACS nano*, 2010, 4, 2429-2437.
26. X. Dong, W. Huang and P. Chen, *Nanoscale Res Lett*, 2011, 6, 60.
27. Y. Chen, Y. Li, D. Sun, D. Tian, J. Zhang and J.-J. Zhu, *Journal of Materials Chemistry*, 2011, 21, 7604-7611.
28. S. J. Daly, G. J. Keating, P. P. Dillon, B. M. Manning, R. O'Kennedy, H. A. Lee and M. R. Morgan, *Journal of Agricultural and Food Chemistry*, 2000, 48, 5097-5104.
29. L. Dunne, S. Daly, A. Baxter, S. Haughey and R. O'Kennedy, *Spectroscopy letters*, 2005, 38, 229-245.
30. Z. Zhang, H. Chen, C. Xing, M. Guo, F. Xu, X. Wang, H. J. Gruber, B. Zhang and J. Tang, *Nano Research*, 2011, 4, 599-611.

31. L. Tang, Y. Wang, Y. Li, H. Feng, J. Lu and J. Li, *Advanced Functional Materials*, 2009, 19, 2782-2789.
32. M. Watt-Smith, J. Friedrich, S. Rigby, T. Ralph and F. Walsh, *Journal of Physics D: Applied Physics*, 2008, 41, 174004.
33. T. Ahmad, I. A. Wani, J. Ahmed and O. A. Al-Hartomy, *Applied Nanoscience*, 2014, 4, 491-498.
34. C. Singh, S. Srivastava, M. A. Ali, T. K. Gupta, G. Sumana, A. Srivastava, R. Mathur and B. D. Malhotra, *Sensors and Actuators B: Chemical*, 2013.
35. A. Kaushik, P. R. Solanki, K. Kaneto, C. Kim, S. Ahmad and B. D. Malhotra, *Electroanalysis*, 2010, 22, 1045-1055.
36. A. Kaushik, A. Vasudev, S. K. Arya, S. K. Pasha and S. Bhansali, *Biosensors and Bioelectronics*, 2013.
37. D. C. Marcano, D. V. Kosynkin, J. M. Berlin, A. Sinitskii, Z. Sun, A. Slesarev, L. B. Alemany, W. Lu and J. M. Tour, *ACS Nano*, 2010, 4, 4806-4814.
38. B. Gao, G. Z. Yue, Q. Qiu, Y. Cheng, H. Shimoda, L. Fleming and O. Zhou, *Advanced materials*, 2001, 13, 1770-1773.
39. S. Srivastava, P. R. Solanki, A. Kaushik, M. A. Ali, A. Srivastava and B. Malhotra, *Nanoscale*, 2011, 3, 2971-2977.
40. P. Kalita, J. Singh, M. Kumar Singh, P. R. Solanki, G. Sumana and B. Malhotra, *Applied physics letters*, 2012, 100, 093702-093702-093704.
41. A. Sharma, Z. Matharu, G. Sumana, P. R. Solanki, C. Kim and B. Malhotra, *Thin Solid Films*, 2010, 519, 1213-1218.
42. J. H. Owino, O. A. Arotiba, N. Hendricks, E. A. Songa, N. Jahed, T. T. Waryo, R. F. Ngece, P. G. Baker and E. I. Iwuoha, *Sensors*, 2008, 8, 8262-8274.
43. S. Piermarini, L. Micheli, N. Ammida, G. Palleschi and D. Moscone, *Biosensors and Bioelectronics*, 2007, 22, 1434-1440.

Figure captions

Fig.1. Schematic representation of immunosensor fabrication.

Fig.2. Transmission electron micrograph of (i) graphene oxide (ii) Au@rGO and (iii) High resolution transmission electron micrograph (HR-TEM) of Au nanoparticle (iv) particle size distribution of Au nanoparticles on rGO sheet.

Fig.3. Scanning electron micrograph of electrophoretically deposited (i) rGO/ITO film (ii) Au@rGO /ITO film (iii) enlarged view of the Au@rGO /ITO film and (iv) antibody functionalized anti-AFB_1/ Au@rGO /ITO film.

Fig.4 (i) UV-Visible spectra of (a) GO (b) rGO and (c) in situ synthesized Au@rGO, inset: UV-Visible spectrum of Au NP showing its characteristic absorption peak at 530 nm (ii) X-Ray photoelectron spectra (XPS) of the C1s region of Au@rGO deconvoluted into characteristic peaks. (iii) Fourier- transform infrared spectra of (a) rGO/ITO (b) Au@rGO /ITO and (c) anti-AFB1/ Au@rGO /ITO.

Fig.5 (i) Cyclic voltammetry of the fabricated (a) GO/ITO, (b) rGO/ITO (c) Au@rGO /ITO, (d) anti-AFB1/ Au@rGO /ITO and (e) BSA/anti-AFB1/ Au@rGO /ITO electrodes obtained using three electrode system in PBS (pH 7.4) containing 5mM [Fe(CN)6]3-/4- at 30 mV/s scan rate. (ii) Cyclic voltammetry of the (a) rGO/ITO (b) Au@rGO 1/ITO (c) Au@rGO /ITO and (d) Au@rGO 2 /ITO electrodes. The concentration of HAuCl4 has been taken as 0.2 mg/mL for Au@rGO 1, 0.4 mg/mL for Au@rGO and 0.8 mg/mL for Au@rGO 2 during the nanocomposite formation; Inset (ii) indicates the variation of anodic peak current of different nanocomposite electrodes as a function of HAuCl4 concentration.

Fig. 6 (i) Electrochemical sensing response of BSA/anti-AFB1/ Au@rGO /ITO electrode obtained as a function of AFB1 concentration (0.1–12 ng mL-1 (ii) Linear calibration plot of the immunoelectrode as a function of AFB1 concentration (curve a); control experiment in absence of antibody (curve b).

Fig. 7 (i) Current response of BSA/anti-AFB_1/ Au@rGO /ITO electrode as a function of time (week) and (ii) Current response of five different BSA/anti-AFB_1/Au@rGO/ITO immunoelectrodes fabricated using the same set of procedure in presence of 1 ng/mL AFB_1 concentration.

Figures

Figure 1

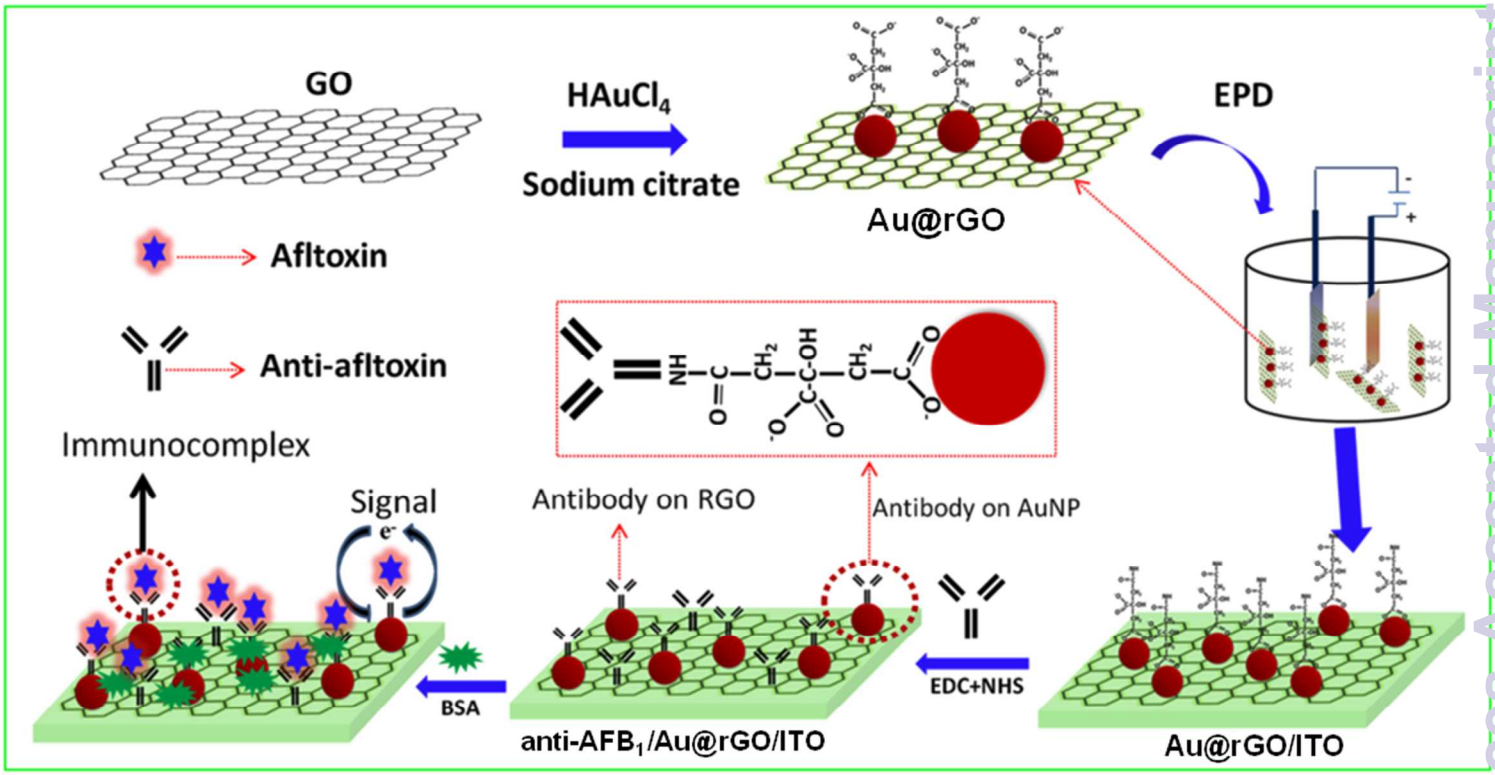

Figure 2

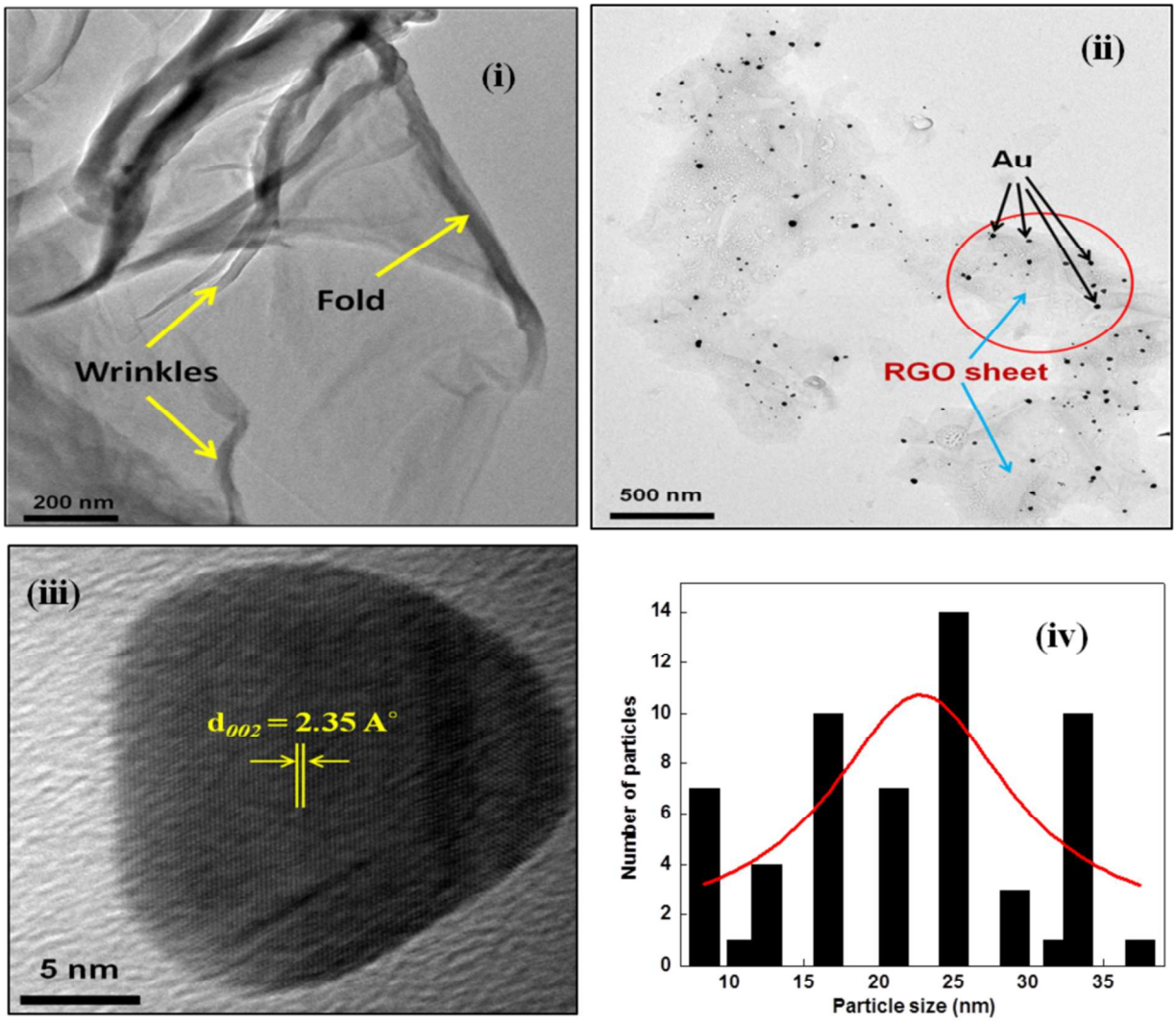

Figure 3

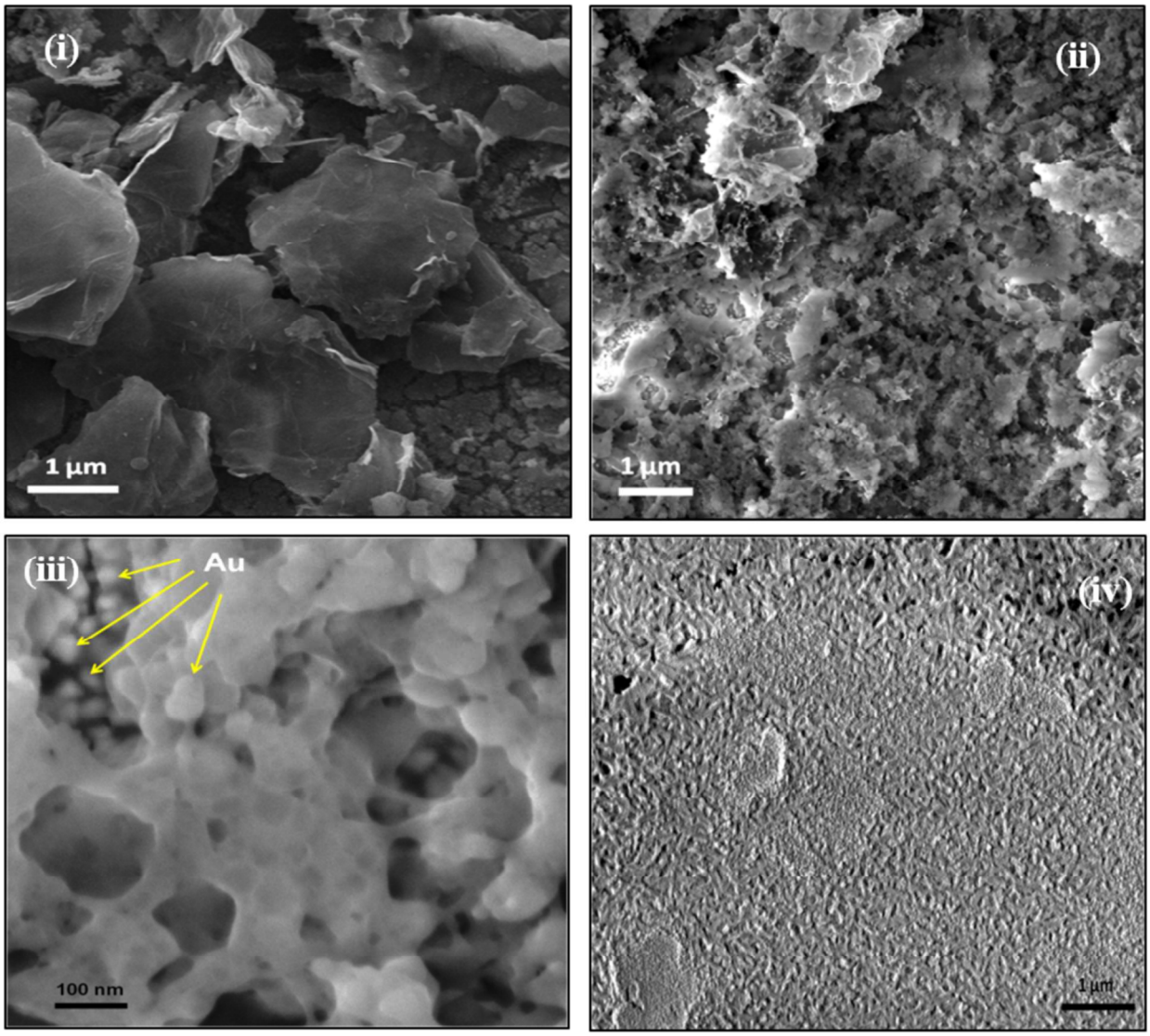

Figure 4

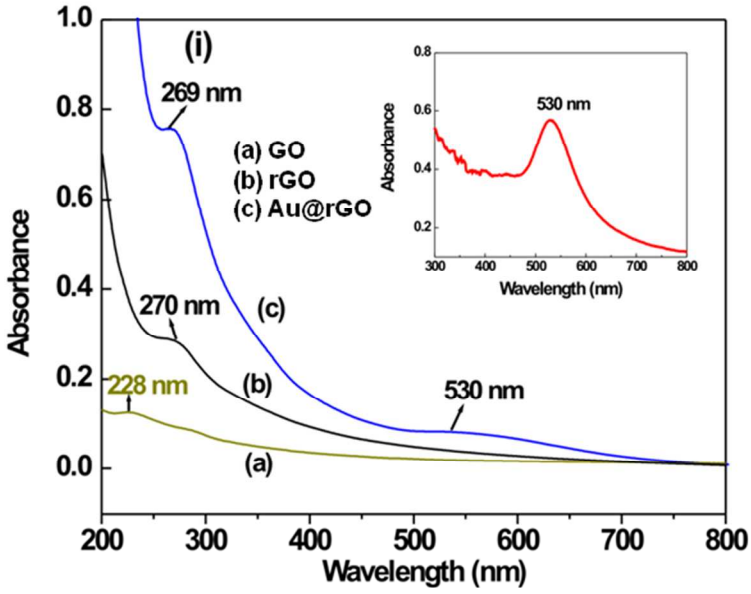

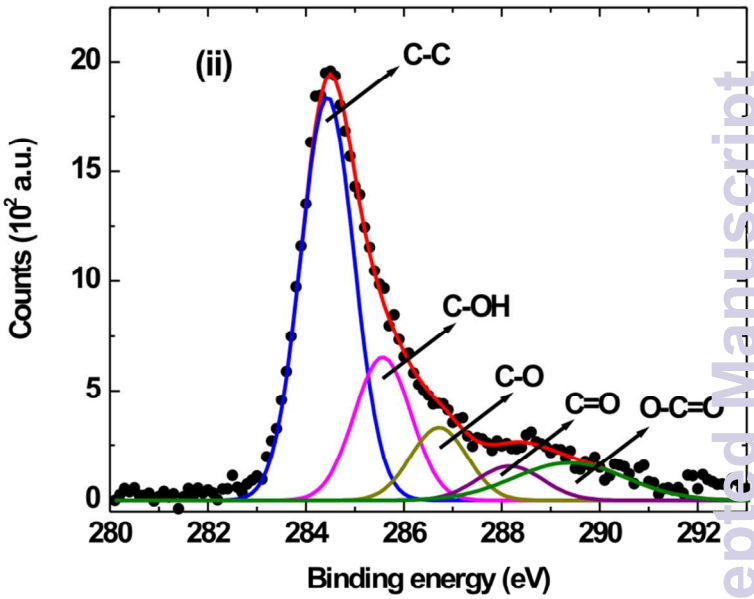

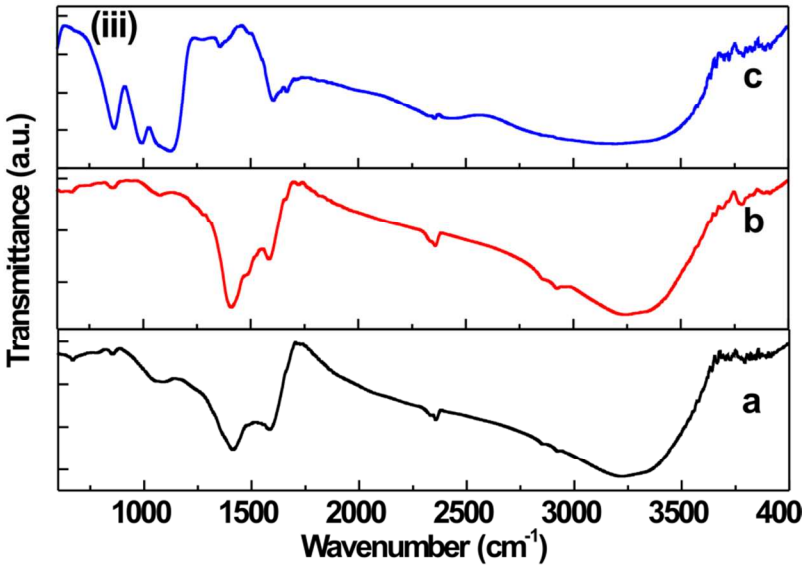

Figure 5

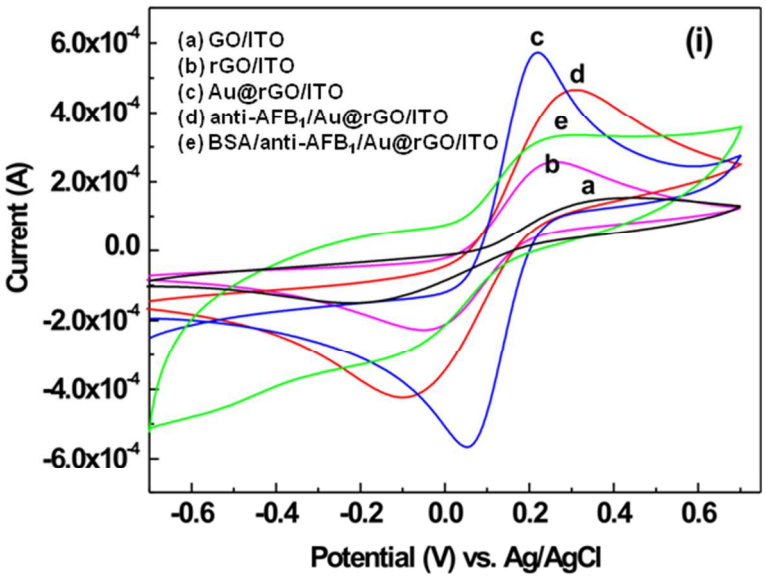

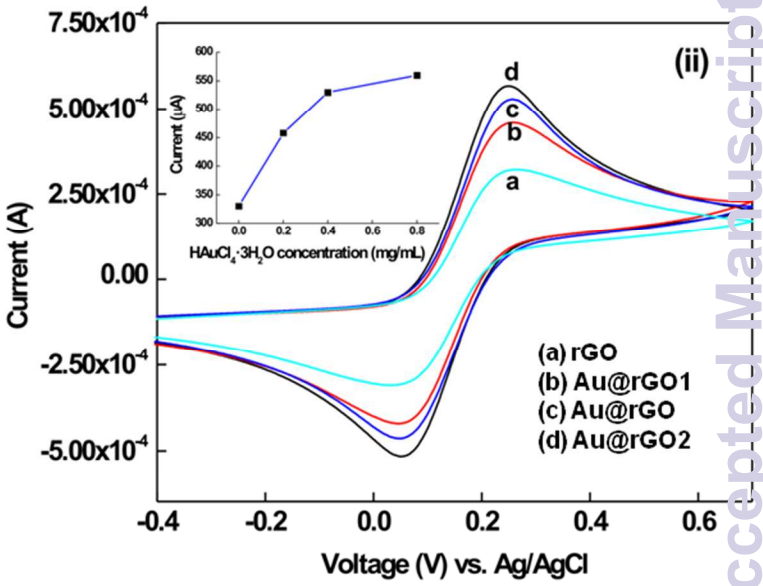

Figure 6

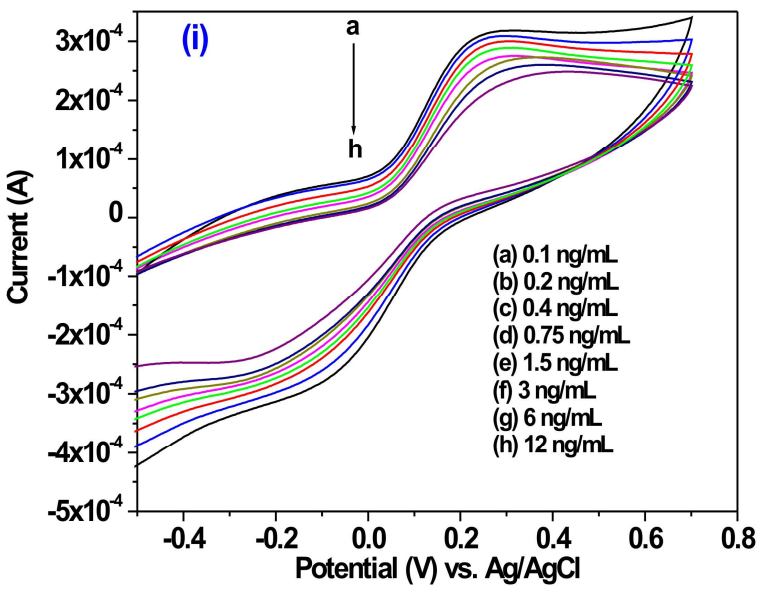

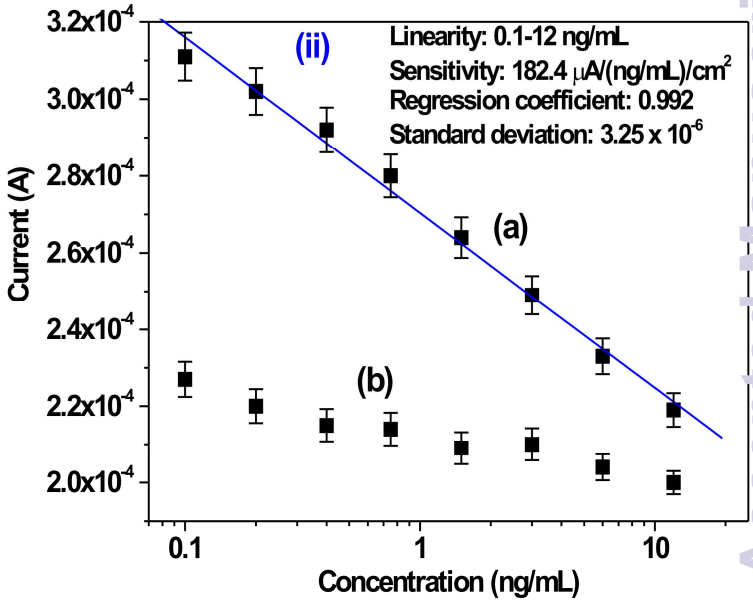

Figure 7